photonics

MDPI

Article

Model-Based Wavefront Correction for Adaptive Multi-Aperture Fiber Coupling Array

Huizhen Yang [1,2], Xianshuo Li [1], Yongqiang Miao [2], Chen Sun [1], Quanyi Ye [1] and Zhiguang Zhang [2,*]

[1] School of Network & Telecom Engineering, Jinling Institute of Technology, Nanjing 211169, China
[2] School of Electronic Engineering, Jiangsu Ocean University, Lianyungang 222005, China
* Correspondence: zhangzhiguang10@mails.ucas.ac.cn

Abstract

The Adaptive Fiber Coupler (AFC) array is an innovative device designed to achieve the stable and efficient coupling of free-space light into optical fibers. To mitigate the effects of atmospheric turbulence, the Stochastic Parallel Gradient Descent (SPGD) algorithm has been predominantly adopted as the control method for AFC systems. However, due to the dynamic nature of atmospheric turbulence, the relatively slow convergence speed of the SPGD algorithm poses significant challenges for practical applications. This paper presents a model-based AFC control system that effectively mitigates wavefront aberrations caused by atmospheric turbulence. The performance of this system was evaluated in comparison with the SPGD algorithm under different turbulence levels and different sub-aperture numbers. Results show that the model-based AFC system converges faster than the SPGD-based AFC system under identical conditions. Additionally, the number of iterations required by the model-based AFC system remains relatively stable, whereas the SPGD-based AFC system demonstrates substantial variability depending on the number of sub-apertures and turbulence levels. As the turbulence level increases, the SPGD-based AFC system requires a greater number of iterations to achieve convergence. The proposed model-based method offers a robust and efficient solution for adaptive multi-aperture fiber coupling systems, which provides theoretical and technical support for the practical application of AFC array.

Keywords: adaptive optics; fiber coupling efficiency; model-based control; multi-aperture system; wavefront correction

1. Introduction

With the continuous advancement of laser communication technology, which integrates the advantages of both radio frequency and optical fiber communications, its applications have substantially broadened to encompass satellite communication [1], terrestrial communication [2], and space communication [3]. In comparison with conventional wireless communication technologies, free-space laser communication technology demonstrates superior attributes such as enhanced resistance to interference, faster data transmission rates, heightened security protocols, a more compact design, and significantly greater information capacity. As a result, it has increasingly become a focal area in wireless communication research.

Constrained by nonlinear effects, thermal mode instability, and the risk of thermal damage, achieving both high power and excellent beam quality with a single fiber poses significant challenges in free-space laser communication technology. To address these

Check for updates

Received: 13 November 2025
Revised: 22 February 2026
Accepted: 24 February 2026
Published: 26 February 2026

Copyright: © 2026 by the authors. Licensee MDPI, Basel, Switzerland. This article is an open access article distributed under the terms and conditions of the Creative Commons Attribution (CC BY) license.

limitations, the coherent combining technology of fiber laser arrays has been proposed [4,5]. This approach substitutes the traditional single-aperture transmission method with an array of smaller apertures, thereby enabling Adaptive Optics (AO) capabilities. Additionally, the development of the Adaptive Fiber Optic Collimator (AFOC) has provided a device for correcting tip/tilt aberrations [6,7]. The AFOC offers several advantages, including its compact size, high bandwidth, and ease of integration. According to the principle of optical path reversibility, the AFOC can also be used as a beam receiver to correct tip/tilt aberrations in real time to achieve efficient and stable single-mode fiber coupling, known as the Adaptive Fiber Coupler (AFC) [8,9]. As a critical component in free-space optical communication systems, the fiber coupler facilitates signal coupling and distribution between fibers. Subsequently, the laser signal is transmitted to the fiber receiving end. The overall performance of the fiber receiving end, including the fiber coupler, represents the performance of the laser communication system. Adaptive multi-aperture fiber coupling arrays, i.e., AFC arrays are designed to achieve stable, high-efficiency coupling of turbulence-distorted free-space optical beams into fiber systems by partitioning the receiver aperture into multiple sub-apertures and applying adaptive control to each channel to mitigate wavefront distortions. From a system-level perspective, an AFC array can be viewed as a phased-array optical receiver, in which multiple spatially separated sub-apertures are jointly optimized to maximize the overall fiber-injected power. This architecture is relevant to a broad range of applications, including satellite-to-ground optical communications, quantum key distribution, coherent optical reception and beam combining, fiber-fed astronomical spectroscopy, and other distributed-aperture optical systems that demand reliable coupling of aberrated free-space beams into fiber networks.

Currently, to overcome the effects of atmospheric turbulence, the Stochastic Parallel Gradient Descent (SPGD) algorithm is predominantly utilized as the control method for AFC systems [10–13]. However, the dynamic characteristics of atmospheric turbulence [14,15] present a significant challenge due to the relatively slow convergence speed of the SPGD algorithm, which hinders practical applications. It requires extensive experimental data and numerous iterative processes to achieve convergence. To enhance the performance of laser communication systems, it is imperative to develop faster control methods that enable AFC systems to rapidly identify optimal control parameters, thereby improving fiber coupling efficiency. Model-based AO control algorithms represent a promising approach for achieving rapid convergence in AFC systems. These methods leverage system models as prior information for designing control algorithms [16–18], theoretically enabling faster convergence rates compared to model-free algorithms.

This paper proposes the application of model-based AO technology, as described in [18], to adaptive multi-aperture fiber coupling control. Compared with SPGD algorithm [19,20], the convergence speed of AFC system and the improvement of the coupling efficiency of optical fiber receiving end are investigated under different turbulence levels and different sub-aperture numbers. The structure of this paper is organized as follows: Section 2 provides an overview of the architecture of AFC and the corresponding laser receiving system. Section 3 details the model-based AFC control method. Sections 4 and 5 present an analysis and discussion of the simulation results. Finally, Section 6 summarizes the conclusions.

2. System Scheme

2.1. Adaptive Fiber Coupler

An optical fiber coupler enables the splitting and combining of optical fields, forming a fundamental building block for fiber-based coupling and combining systems. It finds extensive applications in laser communication, quantum communication, and optical fiber

communication networks. By employing an adaptive fiber coupler, the position and angle of the fiber input can be dynamically adjusted in real-time, thereby achieving efficient reception of spatial optical signals, significantly reducing signal loss, and enhancing system performance and stability.

Figure 1 illustrates the structure of the fiber coupler, which mainly includes a base, bimorph actuators, a cross beam, and a coupling lens. When an external voltage is applied, two pairs of opposing dual piezoelectric actuators drive the cross beam to perform translational movements along the X and Y directions within the rear focal plane of the coupling lens. Consequently, this movement causes the fiber tip, which traverses through the central circular aperture of the cross beam, to shift accordingly, thereby facilitating optical coupling at diverse focal plane positions.

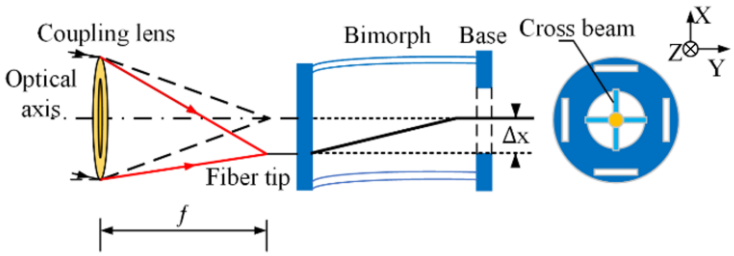


Figure 1. Schematic diagram of the fiber coupler.

The AFC augments the basic fiber coupler (Figure 1) by incorporating a closed-loop control system. This system first detects the centroid position of the intensity distribution, then calculates the necessary adjustment parameters using a control algorithm, and converts these parameters into control signals. After high-voltage amplification, the control signals are applied to the dual piezoelectric actuators, causing them to deform. Consequently, the two pairs of dual piezoelectric actuators can precisely move the fiber tip within the X/Y plane to ensure optimal optical coupling across the entire focal plane.

As the turbulence level increases, the performance of single-channel AFC on the coupling efficiency of single-mode fibers becomes limited. An array-based receiving configuration is recommended to address this limitation [21]. Prior research has theoretically analyzed the coupling characteristics of spatial light into single-mode fiber arrays and demonstrated that, compared to single-channel coupling, array coupling can substantially enhance reception efficiency [22,23].

Therefore, integrating AFC devices with array receiving technology is anticipated to significantly improve the coupling performance of optical receivers in space laser communication systems.

2.2. Adaptive Fiber Coupler Array

The AFC array with control system is illustrated in Figure 2. This system comprises an AFC array, single-mode fibers, photo-detectors, a controller, and a high-voltage amplifier.

The incident wavefront, which contains aberrations, is divided into multiple sub-beams by sub-apertures of AFC. These sub-beams are subsequently focused through the coupling lens. Assuming that the main optical axis of the AFC array aligns approximately with the wave vector of the incident wavefront, a portion of the beam will be coupled into the single-mode fiber at the rear focal plane of the coupling lens. The multi-coupled beams are transmitted via the single-mode fibers to the photo-detectors, where they are converted into electrical signals. The controller receives and processes these electrical signals, then calculates the required voltage signals for actuating the AFC array according to the control algorithm. The voltage signals, after being amplified by the high-voltage amplifier, are

applied to the dual piezoelectric drivers of the AFC array, causing the fiber tip to move at the rear focal plane of the respective coupling lens to achieve optimal coupling efficiency.

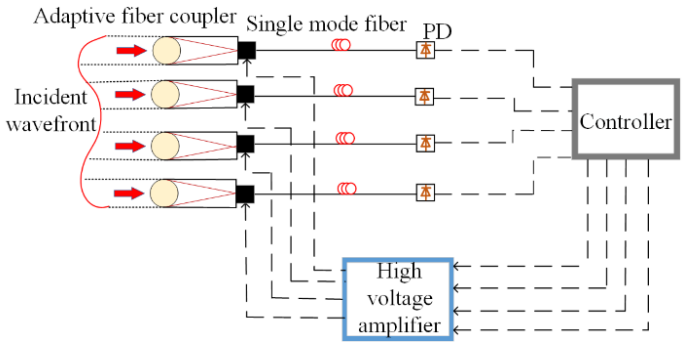


Figure 2. Schematic diagram of AFC array with control system.

According to the aforementioned principle, the controller within the AFC array generates control signals for the dual piezoelectric actuators based on the information acquired by the photodetector. This ensures precise regulation of the fiber tip displacement in the X/Y direction, thereby maintaining high coupling efficiency of the AFC system. Consequently, the control algorithm plays a critical role in determining performance of the AFC system. Given that AFC is predominantly utilized in laser communication through atmospheric transmission environments, it is imperative that the control algorithm not only guarantees optimal coupling efficiency but also ensures adequate convergence speed to enhance adaptability to atmospheric turbulence. We propose to implement the control of AFC systems using the fast model-based AO technology.

3. Model-Based AFC Control Method

3.1. Basic Principles

The change in the masked intensity distribution within the focal plane is proportional to the integral of the square of the phase derivative multiplied by the pupil function for both point sources and extended sources. This relationship has been established based on optical and mathematical analysis, demonstrating that the mean square of the wavefront gradients is approximately linear with respect to the masked focal-plane signal [17,18]. The formula can be expressed as follows:

$$MDS = MDS_0 - \frac{1}{4\pi^2} MSG, \tag{1}$$

where MDS and MSG are the acronyms for Masked Detector Signal and Mean Square Gradient, respectively. MDS_0 is the value of MDS when there is no aberration. Equation (1) accurately describes the linear relationship between MDS and MSG. According to this formula, the value of MDS is always less than 1 and gradually decreases as the aberration increases, reaching a maximum value in the absence of aberration. MDS and MSG are defined as follows:

$$MDS = \frac{\iint I(u,v)\left(1 - \frac{r^2}{R^2}\right) dudv}{\iint I(u,v) dudv}, \tag{2}$$

where $I(u,v)$ is the focal plane intensity distribution, and $1 - r^2/R^2$ is the mask, where $r = \sqrt{u^2 + v^2}$. In practice, the mask could be implemented by the weighting of pixels within the software when the photodetector is replaced by a CCD or CMOS camera.

$$MSG = \frac{\iint_{R^2} P(x,y)\left(\left(\frac{\partial\phi(x,y)}{\partial x}\right)^2 + \left(\frac{\partial\phi(x,y)}{\partial y}\right)^2\right)dxdy}{\iint_{R^2} P(x,y)dxdy}, \tag{3}$$

where (x,y) is the coordinate on the wavefront plane, $P(x,y)$ is the pupil, and $\phi(x,y)$ is the wavefront aberration. The illumination is assumed to originate from a remote point source, resulting in a planar incident wavefront at the entrance pupil. It should be noted that the mean square of the wavefront gradients defined in Equation (3) is always non-negative and does not contain directional information, as it characterizes the magnitude of wavefront distortions rather than the sign of the tilt components. It should also be noted that the linear relationship between the MDS and MSG holds under moderate phase perturbations. Under strong turbulence, the focal-plane intensity becomes increasingly speckle-dominated, leading to larger dispersion and reduced linearity in the $MSG - MDS$ mapping. Numerical evaluation under strong turbulence conditions ($D/r_0 > 10$) shows that the relative approximation error remains within approximately 10% for the perturbation amplitudes used in this work.

The closed-loop control method is designed according to Equation (1), as outlined below. First, the corresponding MDS of the initial wavefront aberration is calculated according to Equation (2), and recorded it as MDS_{Init}. N orthogonal modes are taken as predetermined base functions and are added by the wavefront corrector sequentially with coefficient α to the wavefront aberration. Then corresponding $MDS_1, \ldots, MDS_N$ are obtained. Control parameters V can be estimated [17] by

$$V = [S^{-1}(\frac{1}{4\pi^2}M - \alpha^2 S_m)]/(2\alpha) \approx \frac{S^{-1}M}{2\alpha}, \tag{4}$$

where

$$M = -\begin{Bmatrix} MDS_1 - MDS_{Init} \\ MDS_2 - MDS_{Init} \\ \cdots \\ MDS_N - MDS_{Init} \end{Bmatrix}. \tag{5}$$

The control vector V is then directly applied to actuators, generating the corresponding tip/tilt compensation and updating the wavefront for the next iteration. Here, α represents the physical perturbation amplitude applied to actuators of AFC system when each orthogonal basis mode is introduced. The matrix S, short for MSG, is the second moment of the wavefront gradients. The matrix S^{-1} and the vector S_m are the inverse matrix and the diagonal vector of matrix S respectively. S can be calculated by base functions according to the following equation:

$$S(i,j) = R^{-1}\iint_{R^2}\left[\frac{\partial}{\partial x}F_i(x,\mathrm{y})\frac{\partial}{\partial x}F_j(x,\mathrm{y}) + \frac{\partial}{\partial y}F_i(x,\mathrm{y})\frac{\partial}{\partial y}F_j(x,\mathrm{y})\right]dxdy, \tag{6}$$

where $F(x,y)$ is predefined bias functions. Here, the bias functions refer to the predefined orthogonal basis functions used for wavefront modulation, such as low-order Zernike modes. The tip and tilt mode of Zernike polynomials are used in the application of the AFC system.

3.2. Implementation of Model-Based AFC Array

As shown in Figure 2, the wavefront aberrations degraded by atmospheric turbulence is projected onto the receiving aperture of the AFC array and subsequently divided into multiple sub-beams via the sub-apertures of the fiber coupler array. These sub-beams are then focused through their respective coupling lenses to form multiple focal spots in the rear focal plane. Obviously, the control of the AFC array exhibits the following characteristics. Firstly, multiple sub-aperture channels are controlled independently in parallel, resulting in multiple control loops. Secondly, after segmentation of the wavefront aberrations, each sub-aperture primarily handles the correction of tip/tilt in X and Y directions. Thirdly, when the number of sub-apertures of the AFC array is L, the total number of control parameters becomes $2L$.

It is worth noting that in scenarios with high turbulence levels, each sub-channel must correct higher-order aberrations in order to improve coupling efficiency. Considering the design and fabrication complexities associated with AFC arrays, we focus on correcting the tip/tilt aberrations in two directions for each channel. Based on the aforementioned analysis, when employing model-based AO techniques for AFC array control, the base function $F(x, y)$ in Equation (6) encompass two modes corresponding to the tip/tilt.

When a unit voltage is applied to actuators in either the X or Y direction, the fiber tip will experience displacement in the corresponding direction. Changes in the fiber tip within the XY plane are illustrated in Figure 3. These two patterns serve as base functions of the control algorithm. Owing to the uniformity in process design and manufacturing, these two modes are applicable to all channels of the AFC array.

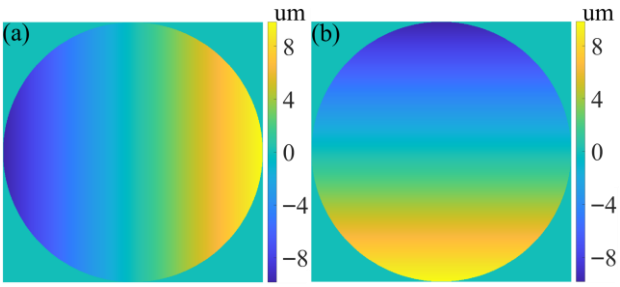


Figure 3. Two base functions of the fiber coupler, where (**a**) is for X direction and (**b**) is for Y direction.

The model-based control algorithm for AFC array can be divided into two parts: the preprocessing step and the iteration step. S and its inverse matrix S^{-1} are calculated according to Equation (6) in the preprocessing step. Matrices S, S^{-1} and vector S_m can be obtained in advance from above two base functions. They do not depend on the wavefront to be corrected. Consequently, the second moment of the wavefront gradients S can be regarded as the prior information of the control algorithm. Here, S is a 2×2 matrix.

One iteration step for one sub-aperture is as follows: obtain the MDS corresponding to the initial wavefront aberration and record it as MDS_{Init} by Equation (2), get MDS_x and MDS_y sequentially through superimposing the base function introduced by dual piezoelectric actuators and write the coefficient vector of base functions as α; compute the control signal V of this iteration according to Equations (4) and (5) and apply V onto actuators; calculate the coupling efficiency η of current sub-aperture of this iteration.

When the AFC system comprises multiple sub-apertures, the control of these sub-apertures is executed in parallel. Following the completion of the current iteration, the overall system coupling efficiency can be derived from the sub-aperture coupling efficiencies, serving as the correction outcome for the current iteration.

4. Results and Analysis

4.1. Simulation Conditions

The sub-apertures of the AFC array are arranged in a densely packed, regular hexagonal configuration, with an aperture filling factor of 1. The aperture filling factor is defined as the ratio of the sub-aperture diameter d to the center-to-center spacing l between adjacent sub-apertures. When the filling factor equals 1, we have $d = l$. The number of sub-apertures varies from 1, 7, 19 to 37. The arrangement of sub-apertures is illustrated in Figure 4, where d represents the diameter of the sub-apertures and l denotes the center-to-center distance between adjacent sub-apertures.

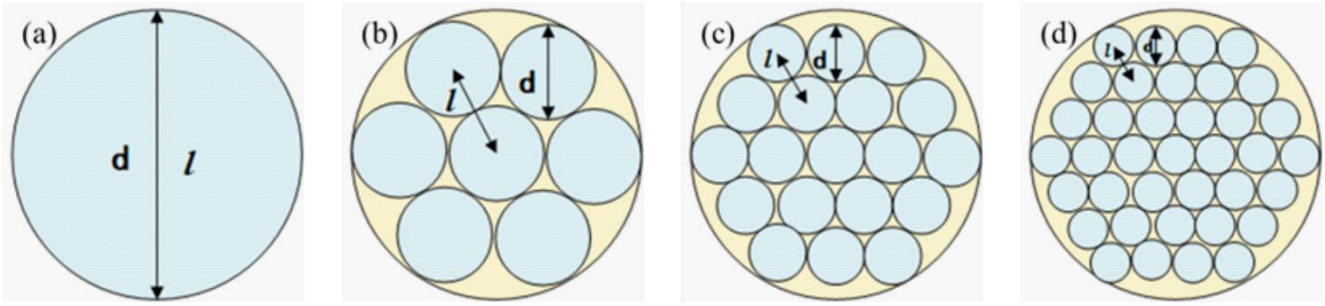


Figure 4. Arrangement of the AFC array, where the equivalent receiving aperture (circle) is fixed. (**a**) N_{sub} = 1. (**b**) N_{sub} = 7. (**c**) N_{sub} = 19. (**d**) N_{sub} = 37.

As illustrated in Figure 4, the spacing between sub-apertures within the array leads to a reduction in the overall received power. Assuming uniform amplitude distribution of light at the receiving aperture, the total coupling efficiency η_{tot} can be expressed as a combination of individual coupling efficiencies η_i (where $j = 1, \ldots, N_{sub}$) according to Equation (7). Here, N_d denotes the maximum number of sub-apertures in the array along the horizontal axis.

$$\eta_{tot} = \frac{1}{N_d^2} \sum_{i=1}^{N_{sub}} \eta_i, \tag{7}$$

When the diameter of sub-aperture d, the mode field radius of single-mode fiber ω_0, and the focal length f of the coupling lens satisfy

$$\pi d\omega_0/(2\lambda f) = 1.12, \tag{8}$$

an optimal single-mode fiber coupling efficiency of 0.81 can be achieved [21,24]. Based on Equation (7), it can be concluded that for the AFC array, when the corresponding sub-aperture numbers N_{sub} are 1, 7, 19, and 37, the maximum overall coupling efficiency η_{tot} values are 0.81, 0.63, 0.62, and 0.61, respectively. The parameters for the simulated fiber coupler are configured as follows: the wavelength λ is set to 1064 nm, the receiving aperture diameter d is 22 mm, the focal length f of the coupling lens is 167 mm, and the mode field radius ω_0 of the single-mode fiber is 5.8 um. These parameters comply with the requirements specified in Equation (8).

The simulation is conducted using MATLAB R2022b. Multi-frame phase screens, corresponding to Kolmogorov's power spectrum under different turbulent levels, are generated through the spectral inversion method of fast Fourier transform combined with low-frequency error compensation. These phase screens serve as input wavefronts at the receiving aperture of the AFC array. The parameter D/r_0 is utilized to quantify the degradation of wavefront aberrations caused by atmospheric turbulence, where D denotes the equivalent receiving aperture of the AFC array. By maintaining D constant, the value of r_0 is adjusted to simulate wavefront aberration changes under different turbulence

levels. Random wavefront aberrations at three different turbulence levels, characterized by D/r_0 of 5, 10 and 15, are selected as correction objects to compare the performance of the model-based method and the SPGD algorithm. The SPGD algorithm employs the total coupling efficiency defined in Equation (7) as its performance metric, and the optimization proceeds by maximizing this metric via gradient descent.

For each turbulence level, 50 random phase screens are corrected, and the average coupling efficiency of the 50-frame phase screens is used as the correction results. Several examples of wavefront aberrations are illustrated in Figure 5, where (a)–(c) corresponds to D/r_0 of 5, 10, and 15, respectively.

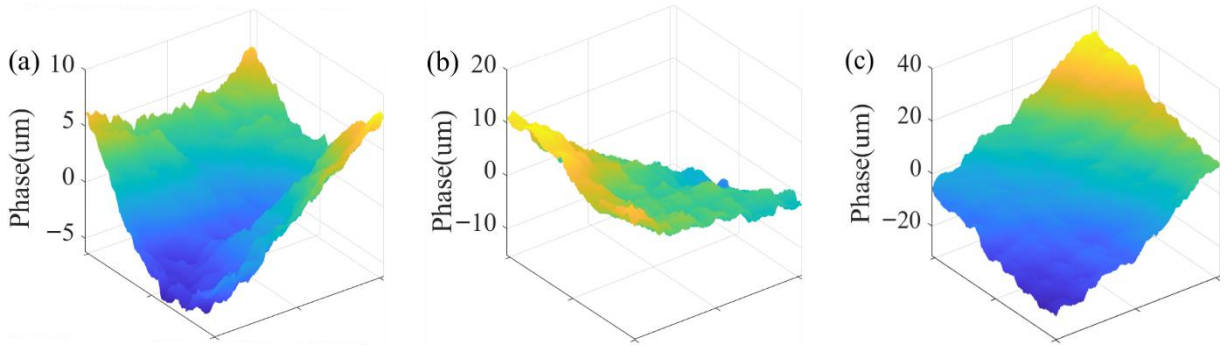


Figure 5. Several examples of wavefront aberrations. (**a**) D/r_0 = 5. (**b**) D/r_0 = 10. (**c**) D/r_0 = 15.

Additionally, when simulating multiple sub-apertures AFC, the focal length f of the coupling lens and the diameter d of the sub-aperture should be correspondingly adjusted while keeping the equivalent receiving aperture D of the AFC array unchanged in order to meet the requirements of Equation (8).

4.2. Array Coupling Efficiency Results and Analysis

During each iteration, both methods require two perturbations: the model-based method applies perturbations sequentially in the X and Y directions, while the SPGD algorithm applies positive and negative perturbations in succession. Consequently, under identical software and hardware conditions and with the same wavefront aberrations, the convergence speed and correction efficacy of the two algorithms can be effectively assessed.

4.2.1. Convergence

Figure 6 illustrates the iterative curves of total coupling efficiency optimized by the SPGD algorithm and the model-based algorithm under different turbulence levels and sub-aperture numbers after 60 iterations. It should be noted that the results corresponding to Figure 6 are obtained under a quasi-static turbulence assumption, where the atmospheric aberration is assumed to remain unchanged during one optimization process. The black, red, and blue lines correspond to D/r_0 values of 5, 10 and 15, respectively. Solid lines with ∇ symbols represent the model-based algorithm, while dashed lines marked with * symbols indicate the SPGD algorithm.

It is evident from Figure 6 that both algorithms achieve convergence after 60 iterations for different turbulence levels and different numbers of sub-apertures. Under identical turbulent conditions for a single aperture, the coupling efficiency achieved using the model-based method is significantly higher than that obtained with the SPGD algorithm, while both methods demonstrate comparable convergence rates. Although the model-based correction markedly enhances the coupling efficiency—for instance, increasing from 0.02 to 0.38 when D/r_0 is 5—it still falls short the theoretical value of 0.81. Based on coupling efficiency, it can be seen that a single aperture can obtain the maximum coupling efficiency

due to the absence of gaps. Nevertheless, these results suggest that the turbulence has a substantial impact on the coupling efficiency of single apertures. Even with the application of adaptive optics technology, the improvement in coupling efficiency remains constrained, thereby highlighting one of the key motivations for proposing fiber coupler arrays in relevant fields.

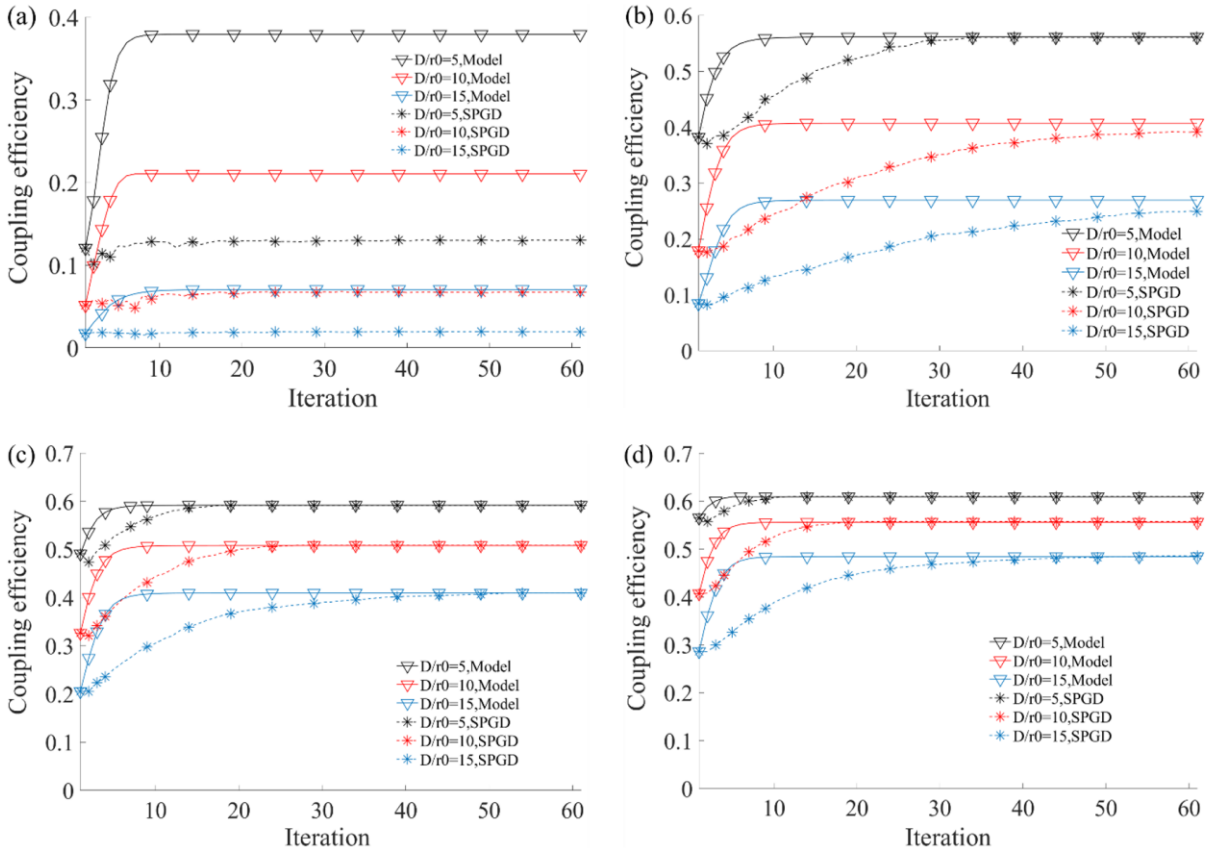


Figure 6. Convergence curves of model-based and SPGD-based AFC systems. (**a**) N_{sub} = 1. (**b**) N_{sub} = 7. (**c**) N_{sub} = 19. (**d**) N_{sub} = 37.

For multiple sub-aperture fiber couplers, the coupling efficiency after correction by two control algorithms is essentially equivalent under the same turbulence levels and numbers of sub-apertures. However, the model-based method exhibits a significantly superior convergence speed compared to the SPGD method. For an AFC system featuring the same number of sub-apertures, when turbulence is weak (e.g., D/r_0 = 5), the coupling efficiency after AO correction approaches the theoretical value. Nevertheless, as the turbulence level increases, the coupling efficiency after correction progressively decreases. Despite this reduction, the coupling efficiency after correction remains markedly higher than before correction. Under the same turbulence level, the higher the number of sub-apertures of AFC, the higher the coupling efficiency after AO correction.

4.2.2. Correction Accuracy

To enable a more systematic visual comparison and analysis of the coupling efficiency of the AFC system before and after correction under different sub-aperture numbers and turbulence levels, the coupling efficiency values are plotted on four separate graphs, as illustrated in Figure 7, where (a)–(d) subfigures are for N_{sub} = 1, 7, 19 and 37, respectively. Green lines and blue lines denote the ideal coupling efficiency and the initial coupling efficiency for different sub-aperture systems under different turbulent levels, respectively. Black and red lines represent the coupling efficiency after correction by the model method

and the SPGD algorithm, respectively. In addition, to further distinguish lines of different colors, different symbols are also used for marking.

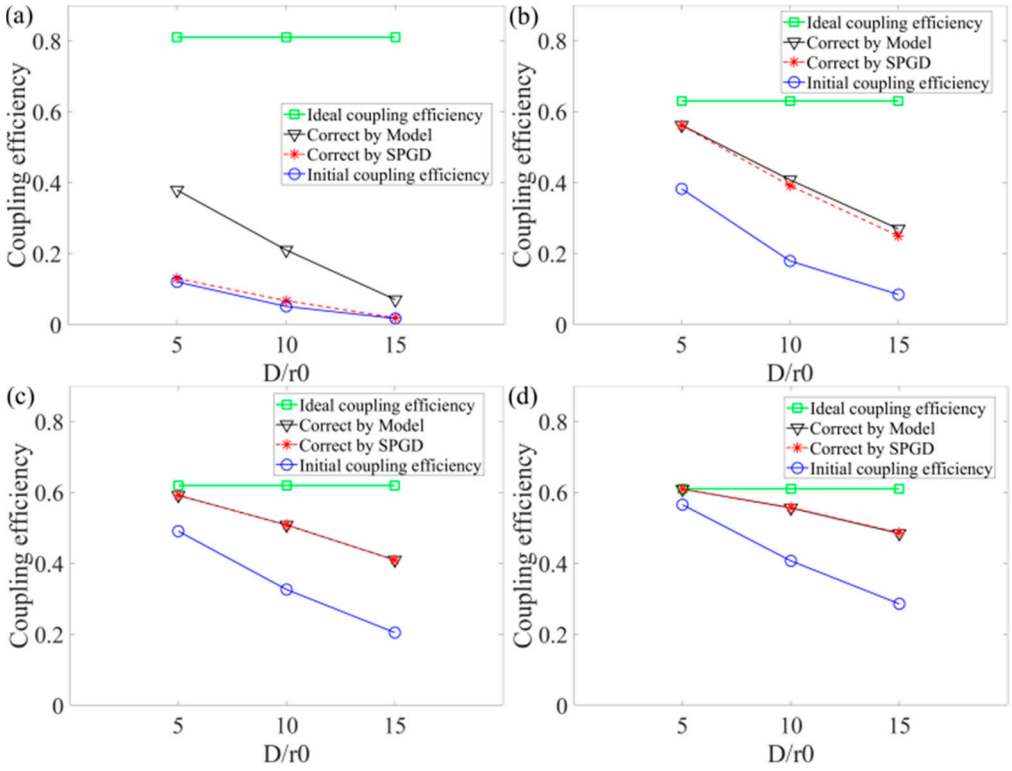


Figure 7. Coupling efficiency of AFC with different numbers of sub-apertures under different turbulence levels before and after correction by two control algorithms. (**a**) N_{sub} = 1. (**b**) N_{sub} = 7. (**c**) N_{sub} = 19. (**d**) N_{sub} = 37.

By comparing the theoretical coupling efficiency in Figure 7, it can be found that the single-aperture theoretical coupling efficiency is the highest, but the initial coupling efficiency under different turbulence conditions is the lowest, indicating that the single-aperture is most affected by turbulence. Under the same turbulence level, the coupling efficiency increases with the number of sub-apertures, validating the rationality for employing sub-aperture arrays instead of single apertures. However, for AFC systems with an identical number of sub-apertures, coupling efficiency significantly diminishes as the turbulence strength increases. For example, when the sub-aperture number is 19, the coupling efficiency decreases from 0.5 at $D/r_0 = 5$ to 0.2 at $D/r_0 = 15$. These analyses further demonstrate the necessity of implementing adaptive optics technology in AFC system.

It is also evident that the coupling efficiency after correction of both control algorithms shows significant improvement under different turbulence levels and different number of sub-apertures in Figure 7. The model-based method demonstrates higher correction accuracy compared to the SPGD algorithm when the number of sub-apertures is fewer than 7. When the number of sub-apertures exceeds 7, the correction accuracy of the two methods becomes comparable. Although neither method achieves the theoretical maximum, the enhancement in coupling efficiency is more pronounced at higher turbulence levels. For instance, when the number of sub-aperture is 19, the coupling efficiency increases from 0.49 to 0.59 at $D/r_0 = 5$; from 0.32 to 0.50 at $D/r_0 = 10$ and from 0.19 to 0.41 at $D/r_0 = 15$.

When the number of sub-apertures exceeds 19, the corrected coupling efficiency of both algorithms approaches the theoretical value under low turbulence level (e.g., $D/r_0 = 5$) from Figure 7c,d. However, under higher turbulence levels (e.g., $D/r_0 = 15$), the coupling efficiency increases from 0.28 to 0.48 for 37 sub-aperture system, which is

very close to 19 sub-aperture system. These findings indicate the necessity of incorporating high-frequency wavefront correction in strong turbulent levels. However, it is important to note that for a given equivalent aperture D, an increase in the number of sub-apertures leads to higher design and manufacturing costs as well as increased technical complexity. Considering cost and technical feasibility, it is recommended to use AFC arrays with 7 or 19 sub-apertures in practical applications.

4.2.3. Correction Speed

The convergence speed of the control algorithm is quantified by the number of iterations required for AFC system convergence. Using 80% of the correction range achieved by the model-based method as a benchmark, we assess the number of iterations required for each algorithm to meet this criterion under different sub-aperture numbers and different turbulent levels. In addition, in order to be more practical, we compare the number of iterations required for convergence of multiple sub-aperture systems, and do not consider single aperture systems. The comparison results are shown in Figure 8, where the red symbols represent the model-based method, and the black symbols correspond to the SPGD method.

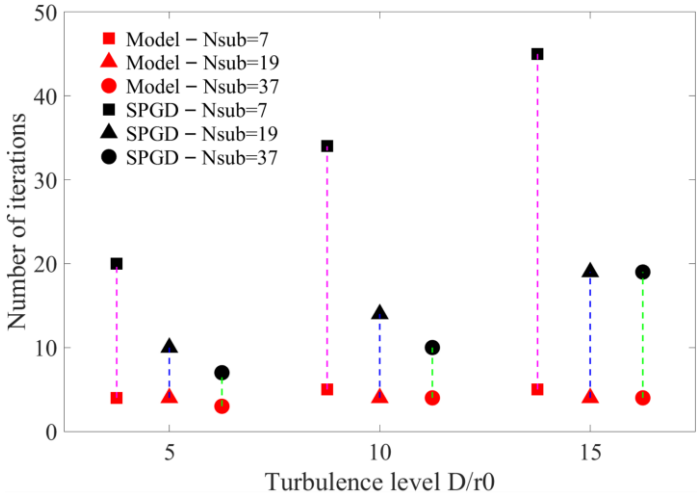


Figure 8. Comparison of iteration number needed by model-based AFC and SPGD-based AFC under different sub-aperture numbers and turbulence levels.

As illustrated in Figure 8, the model-based AFC system requires fewer iterations than the SPGD-based AFC system under different turbulence levels and different sub-aperture numbers. The correction speed of the model-based AFC system outperforms the SPGD-based AFC system, achieving a speed improvement of more than twofold while maintaining higher stability. Moreover, it is noteworthy that the number of iterations required by the model-based AFC system remains relatively stable regardless of changes in turbulence levels or sub-aperture numbers. In contrast, the number of iterations for the SPGD-based AFC system increases with higher turbulence levels. Figure 8 also reveals that when the number of sub-apertures is 7, the SPGD-based AFC system requires significantly more iterations at different turbulence levels compared to configurations when the number of sub-apertures is 19 or 37. This discrepancy is primarily attributed to the lower initial coupling efficiency with 7 sub-apertures.

When the AFC system is utilized in the laser communication through atmosphere turbulence channel, the convergence speed of the control algorithm becomes a critical factor due to the stochastic wavefront aberrations induced by atmospheric turbulence. Based on the aforementioned analysis, the model-based method demonstrates relatively stable

convergence rates under different turbulence levels and different sub-aperture numbers. In contrast, the SPGD algorithm necessitates more iterations as turbulence strength increases. For instance, with 19 sub-apertures, each of the three turbulence levels requires only 5 iterations for the model-based method, whereas the SPGD algorithm demands 10, 14, and 19 iterations, respectively. It should be noted that the simulations are conducted under a frozen turbulence assumption, where the wavefront remains unchanged during each optimization process. Under this condition, both the model-based method and the SPGD algorithm operate within a correction cycle that is effectively faster than the turbulence variation, while the significantly reduced iteration number of the model-based method indicates its stronger potential for real-time implementation.

5. Discussion

This section discusses the underlying mechanisms and practical implications of the proposed model-based wavefront sensorless control method, focusing on its convergence behavior, robustness under different turbulence conditions, and scalability with respect to the number of sub-apertures. The essential difference between the proposed model-based method and the SPGD algorithm lies in their optimization mechanisms. In Figure 8, SPGD requires more iterations for 7 sub-apertures than for 19 or 37, primarily due to the lower initial coupling efficiency. Starting from a lower-efficiency state, the system requires more iterations to converge, whereas the higher initial efficiency of 19 and 37 sub-apertures allows faster convergence. Moreover, SPGD relies on random perturbations to estimate the gradient, and a starting state closer to the target enhances the effectiveness of each perturbation, further accelerating convergence. In contrast, the model-based method demonstrates stable and efficient convergence across different sub-aperture numbers, providing a robust solution for multi-aperture adaptive fiber coupling systems.

The model-based method exploits an explicit and deterministic relationship between the masked detector signal (MDS) and the wavefront mean square gradient (MSG). By introducing predefined orthogonal perturbations with known amplitudes and directly estimating the aberration coefficients through a linear model, the control process avoids stochastic searching. As a result, the correction speed is largely decoupled from both turbulence strength and the number of sub-apertures, which explains the stable iteration count observed in the simulation results.

The MSG–MDS linear relationship is adopted as a first-order approximation, which is generally reliable in weak to moderate turbulence. As turbulence becomes stronger, higher-order aberrations and speckle-dominated intensity fluctuations increase the dispersion and nonlinearity of the MSG–MDS mapping, and the quantitative accuracy of the linear model may degrade. Nevertheless, within the turbulence regimes investigated in this study, the MSG–MDS relationship remains sufficiently accurate to serve as a reliable model. Numerical evaluations indicate that, even for strong turbulence regimes ($D/r_0 > 10$), the approximation error remains sufficiently small for control purposes. Moreover, the estimation of control parameters is completed through a finite and deterministic sequence of measurements rather than iterative performance metric optimization, further enhancing stability.

It should be noted that the convergence behavior presented in this study is obtained under a quasi-static turbulence assumption, where atmospheric aberrations remain approximately constant during one optimization cycle. Under this assumption, the model-based method is able to reconstruct and compensate dominant aberration components before significant temporal decorrelation occurs. Another important observation is that increasing the number of sub-apertures does not significantly affect the number of iterations required by the proposed method. This contrasts with SPGD, whose convergence speed generally

decreases with increasing control dimensionality. For the model-based method, control dimensionality mainly influences the computational load associated with parameter estimation, rather than the convergence speed itself, which is particularly advantageous for large-scale adaptive fiber-coupling arrays.

Finally, while the simulation results validate the effectiveness of the proposed approach, several practical considerations should be acknowledged. The linear model assumes small perturbation amplitudes and neglects higher-order nonlinear effects. In real systems, actuator nonlinearities, measurement noise, and finite system bandwidth may also influence estimation accuracy. Nevertheless, the deterministic structure of the proposed method provides a clear framework for incorporating calibration procedures and compensating non-ideal effects in future experimental implementations.

6. Conclusions

Compared to single-channel coupling, array coupling can substantially enhance reception efficiency. However, the coupling efficiency of AFC significantly diminishes as the turbulence strength increases. To mitigate the disturbance of atmospheric turbulence, SPGD algorithm is often used to control AFC system. Nevertheless, due to the dynamic nature of atmospheric turbulence, the relatively slow convergence speed of the SPGD algorithm poses significant challenges for practical applications. In this paper, we propose a model-based adaptive multi-aperture fiber coupling system and evaluates its performance in comparison with SPGD algorithm. The analysis focuses on fiber coupling efficiency under different turbulence levels and different sub-aperture numbers.

Results demonstrate the corrected coupling efficiency of both control algorithms shows significant improvement under different turbulence levels and different numbers of sub-aperture. Specifically, the model-based method demonstrates notably higher correction accuracy compared to the SPGD algorithm, particularly when the number of sub-apertures is fewer than 19. When the number of sub-apertures exceeds 19, the correction accuracy of the two methods becomes comparable. In terms of the rate of convergence, the model-based AFC system outperforms the SPGD-based AFC system, achieving a speed improvement of more than twofold. Moreover, the model-based method demonstrates relatively stable convergence rates under different turbulence levels and different sub-aperture numbers. In contrast, the SPGD algorithm necessitates more iterations as turbulence strength increases. Overall, the proposed model-based method offers a robust and efficient solution for adaptive multi-aperture fiber coupling systems. It enhances system performance by achieving higher accuracy and faster correction speed, making it a valuable approach for mitigating the adverse effects of atmospheric turbulence. Future research will focus on experimental validation of the model-based AFC system under real-world atmospheric turbulence conditions.

Author Contributions: Conceptualization, H.Y. and Z.Z.; methodology, H.Y. and X.L.; software, Y.M.; validation, X.L. and Y.M.; resources, H.Y. and Q.Y.; writing—original draft preparation, X.L. and C.S.; writing—review and editing, H.Y., Z.Z. and Q.Y.; funding acquisition, H.Y. All authors have read and agreed to the published version of the manuscript.

Funding: National Natural Science Foundation of China (12473081 and U2141255); National Laboratory on Adaptive Optics Project (FNLAO-24-MS-O01).

Institutional Review Board Statement: Not applicable.

Informed Consent Statement: Not applicable.

Data Availability Statement: The data presented in this study are available on request from the corresponding author.

Conflicts of Interest: The authors declare no conflicts of interest.

References

1. Jiang, X.; Guo, Y.; Wang, Y. Performance of modulating retro-reflector-assisted ground-HAP-satellite uplink laser communication system. *Appl. Opt.* **2023**, *62*, 9502–9511. [CrossRef]
2. Zhang, J.; Liu, Y.; Gao, S.; Han, C. Control Technology of Ground-Based Laser Communication Servo Turntable via a Novel Digital Sliding Mode Controller. *Appl. Sci.* **2019**, *9*, 4051. [CrossRef]
3. Wang, F.; Hu, G.; Sun, Y.; Hao, X.; Chen, J.; Wu, P. Performance research of mPPM-QPSK modulation signal for free space optical communication. *Opt. Commun.* **2020**, *457*, 124646. [CrossRef]
4. Goodno, G.D.; Mcnaught, S.J.; Eothenberg, J.E.; Mccomb, T.S.; Thielen, P.A.; Wickham, M.G.; Weber, M.E. Active phase and polarization locking of a 1.4 kW fiber amplifier. *Opt. Lett.* **2010**, *35*, 1542–1544. [CrossRef]
5. Yu, C.X.; Augst, S.J.; Redmond, S.M.; Goldizen, K.C.; Murphy, D.V.; Sanchez, A.; Fan, T.Y. Coherent combining of a 4 kW, eight-element fiber amplifier array. *Opt. Lett.* **2011**, *36*, 2686–2688. [CrossRef]
6. Vorontsov, M.A.; Weyrauch, T.; Beresnev, L.A.; Carhart, G.W.; Liu, L.; Aschenbach, K. Adaptive array of phased-locked fiber collimators: Analysis and experimental demonstration. *IEEE J. Sel. Top. Quantum Electron.* **2009**, *15*, 269–280. [CrossRef]
7. Geng, C.; Luo, W.; Tan, Y.; Liu, H.; Mu, J.; Li, X. Experimental demonstration of using divergence cost-function in SPGD algorithm for coherent beam combining with tip/tilt control. *Opt. Exp.* **2013**, *21*, 25045–25055. [CrossRef] [PubMed]
8. Weyrauch, T.; Vorontsov, M.A.; Carhart, G.W.; Simonova, G.V.; Beresnev, L.A.; Polnau, E.E. Adaptive optical antennas: Design and evaluation. *Proc. SPIE 6708 Atmos. Opt.* **2007**, *6708*, 67080R.
9. Luo, W.; Geng, C.; Wu, Y.; Tan, Y.; Luo, Q.; Liu, H.; Li, X. Experimental demonstration of single-mode fiber coupling using adaptive fiber coupler. *Chin. Phys. B* **2014**, *23*, 014207. [CrossRef]
10. Chang, H.; Chang, Q.; Xi, J.; Hou, T.; Su, R.; Ma, P.; Wu, J.; Li, C.; Jiang, M.; Ma, Y.; et al. First experimental demonstration of coherent beam combining of more than 100 beams. *Photonics Res.* **2020**, *8*, 1943–1948. [CrossRef]
11. Weyrauch, T.; Vorontsov, M.; Mangano, J.; Ovchinnikov, V.; Bricker, D.; Polnau, E.; Rostov, A. Deep turbulence effects mitigation with coherent combining of 21 laser beams over 7 km. *Opt. Lett.* **2016**, *41*, 840–843. [CrossRef] [PubMed]
12. Feng, X.; Zhou, W.; Chen, H.; Ma, Y.; Tong, Y. Photonics Breakthroughs 2024: Multidimensional Integrated (de) Multiplexers for Optical Fiber Communications. *IEEE Photonics J.* **2025**, *17*, 7100509. [CrossRef]
13. Zou, F.; Zuo, J.; Geng, C.; Li, F.; Huang, G.; Liu, J.; Jiang, J.; Fan, Z.; Li, X. Adaptive Laser Aiming Through 2 km Horizontal Atmosphere with Precise-Delayed SPGD Algorithm. *J. Russ. Laser Res.* **2021**, *42*, 462–467. [CrossRef]
14. Song, X.; Li, H.; Li, Z.; Li, S.; Wu, Y. Deep optics framework utilizing a liquid crystal microlens array for dynamic wavefront sensing and correction in atmospheric turbulence. *Opt. Lett.* **2025**, *50*, 3584–3587. [CrossRef]
15. Reddy, E.M.; Therese, A.B. Analysis of atmospheric effects on free space optical communication. In Proceedings of the 2017 International Conference on Nextgen Electronic Technologies: Silicon to Software (ICNETS2), Chennai, India, 23–25 March 2017; pp. 338–343.
16. Ren, H.; Dong, B. Improved model-based wavefront sensorless adaptive optics for extended objects using N + 2 images. *Opt. Exp.* **2020**, *28*, 14414–14427. [CrossRef]
17. Lin, H.; Chang, R. Wavefront Sensorless Adaptive Optics: A General Model-based Approach. *Opt. Exp.* **2011**, *19*, 371–379.
18. Yang, H.; Soloviev, O.; Verhaegen, M. Model-based wavefront sensorless adaptive optics system for large aberrations and extended object. *Opt. Exp.* **2015**, *23*, 24587–24601. [CrossRef]
19. Huang, G.; Geng, C.; Li, F.; Yang, Y.; Li, X. Adaptive SMF coupling based on precise-delayed SPGD algorithm and its application in free space optical communication. *IEEE Photonics J.* **2018**, *10*, 7904212. [CrossRef]
20. Feng, L.; Chao, G.; Xin, L.; Wen, L.; Qi, Q. Technical research of adaptive fiber coupler array based on SPGD algorithm. *Infrared Laser Eng.* **2015**, *44*, 2156–2161.
21. Bian, Y.; Li, Y.; Chen, E.; Li, W.; Hong, X.; Qiu, J.; Wu, J. Free-space to single-mode fiber coupling efficiency with optical system aberration and fiber positioning error under atmospheric turbulence. *J. Opt.* **2022**, *24*, 025703–025714. [CrossRef]
22. Gatt, P.; Costello, T.P.; Heimmermann, D.A.; Castellanos, D.C.; Weeks, A.R.; Stickley, C.M. Coherent optical array receivers for the mitigation of atmospheric turbulence and speckle effects. *Appl. Opt.* **1996**, *35*, 5999–6009. [CrossRef] [PubMed]

23. Weeks, A.R.; Xu, J.; Phillips, R.R.; Andrews, L.C.; Stickley, C.M.; Sellar, G.; Stryjewski, J.S.; Harvey, J.E. Experimental verification and theory for an eight-element multiple-aperture equal-gain coherent laser receiver for laser communications. *Appl. Opt.* **1998**, *37*, 4782–4788. [CrossRef] [PubMed]
24. Geng, C.; Li, X.; Shu, B.; Su, R.; Wang, X.; Wang, X.; Xu, X.; Zhou, P. Experimental research of tilt-tip wavefront and phase-locking control in fiber lasers coherent beam combining. *Infrared Laser Eng.* **2013**, *42*, 1443–1447.

Disclaimer/Publisher's Note: The statements, opinions and data contained in all publications are solely those of the individual author(s) and contributor(s) and not of MDPI and/or the editor(s). MDPI and/or the editor(s) disclaim responsibility for any injury to people or property resulting from any ideas, methods, instructions or products referred to in the content.